# *Water recovery from the high salinity brine: Effect of the interlayer structure in the polyamide nanofiltration membrane*

Journal of Environmental Chemical Engineering 12 (2024) 111963

Contents lists available at ScienceDirect

Journal of Environmental Chemical Engineering

journal homepage: www.elsevier.com/locate/jece

# Water recovery from the high salinity brine: Effect of the interlayer structure in the polyamide nanofiltration membrane

Yuyang Wu [a], Chen Yao [a], Yuanyuan Wang [a], Mingmei Ding [a,*], Hang Xu [a,b], Xu Yan [d], Li Gao [c,*]

[a] Ministry of Education Key Laboratory of Integrated Regulation and Resource Development on Shallow Lakes, Hohai University, Nanjing 210098, China
[b] Suzhou Research Institute of Hohai University, Suzhou 215000, China
[c] Institute for Sustainable Industries and Liveable Cities, Victoria University, PO Box 14428, Melbourne, Victoria 8001, Australia
[d] Huizhou Innovation Research Institute of Next Generation Industrial Internet, Huizhou 516006, China

ARTICLE INFO

*Keywords:*
Water recovery
Nanofiltration membrane
Interfacial polymerization
Interlayered thin-film nanocomposite

ABSTRACT

Water recovery by nanofiltration (NF) from the high salinity brine is emerging as a promising technology to alleviate the water shortage. Thin film composite membranes with polyamide (PA) selective layer are the mainstream in the field of NF. Nevertheless, the trade-off between permeance and retention as well as the structural stability of the mainstream PA membrane still restrict their widespread application. Herein, a novel interlayered thin-film nanocomposite (TFNi) nanofiltration membrane was fabricated based on the interfacial polymerization. The PDA@MXene hybrid was employed as the interlayer to modulate the adsorption and diffusion process of amine monomers, giving rise to the formation of thin and rough PA selective layer, which could accelerate the transport of water molecules. Moreover, PM-TFNi membrane demonstrated higher cross-linking degree and more negatively charged surface, significantly benefiting the repulsion of inorganic salt ions. In this context, PM-TFNi membrane rendered a competitive permselectivity with the water flux of 18.3 L $m^{-2}$ $h^{-1}$ $bar^{-1}$ and the $Na_2SO_4$ rejection of 98.0%. In addition, PM-TFNi membrane exhibited distinguished long-term stability and pH resistance. Overall, this work would provide a paradigm shift in designing high-performance and robust NF membrane for the water treatment.

## 1. Introduction

In recent decades, the rapid urbanization and population explosion has led to a critical issue of water scarcity, which has become a major obstacle impeding the development of society and the economy [1,2]. Due to the compelling advantages of high selectivity and low energy consumption, water recovery from the high salinity brine by membrane-based technology has emerged as one of the promising ways to provides an alternative source of fresh water [3,4]. Particularly, nanofiltration technology is usually used to remove multivalent ions organic molecules with molecular weight ranging from 200 to 2000 Da on the basis of size screening effect and Donan effect. Thin film composite (TFC) membrane, as one of the mainstream NF membranes in the commercial market, is commonly fabricated by interfacial polymerization (IP) process, wherein the polyamide (PA) selective layer was formed on the porous substrate through the reaction between the organic amines (such as piperazine) and acyl chlorides (such as trimesoyl chloride) [5–7]. Nevertheless, most advanced TFC membranes still struggle with the trade- off between the permeability and selectivity derived from the undesired structure [8,9]. Therefore, it is indispensable to design the TFC membrane with satisfying PA active layer to realize the optimized nanofiltration performance.

Generally, the physicochemical characteristics of the porous substrates play a crucial role in the IP process, whereby the distributed concentration and diffusion rate of the reacted monomers would be manipulated by modulating surface properties and pore structure of porous substrates, further affecting the formation and growth of PA selective layer [10,11]. Interlayered thin-film nanocomposite (TFNi) membrane provides great opportunity to improve the permeability without the sacrifice of selectivity. In this context, an interlayer is introduced to modified the substrate and further control the IP process, which would regulate the surface morphology, thickness and density of PA layer [12–14]. Two-dimensional materials with lamellar structure and hydrophilic groups have attracted extensive attention as the intermediate layer [15]. On the one hand, it would provide a wider adhesion area for the adsorption of aqueous monomer and facilitate the benefit to

* Corresponding authors.
*E-mail addresses:* dingmm2021@163.com (M. Ding), Li.gao@vu.edu.au (L. Gao).

https://doi.org/10.1016/j.jece.2024.111963
Received 15 May 2023; Received in revised form 18 September 2023; Accepted 14 January 2024
Available online 17 January 2024

the formation of PA layer with thinner and rougher structure. On the other hand, the tortuous channels formed by the layer-stacking nanosheets could offer a potential interface, inhibiting the infiltration of the reactive monomers into substrate pores and further reducing the thickness of PA layer [16]. However, the enhancement in water permeance is still limited due to extra resistance derived from the lamellar layer. Moreover, the structural instability caused by the weak affinity between the interlayer and substrate is also a formidable challenge for real-life application [17].

MXene composed of early transition metal carbides and/or carbonitrides were first discovered in 2011 [18,19]. The laminate structure, large surface area, hydrophilic property and mechanical flexibility endow it with enormous potential in the field of membrane separation [20–22]. $Ti_3C_2T_x$, one of the most widely used MXene, has been deemed to be the applicable alternative as the interlayer to adjust the IP process [23,24]. Dopamine featuring with bio-inspired stickiness through self-polymerization has been extensively employed for the multifunctional material surface coating [25–27]. Polydopamine (PDA) would provide reactive groups to strengthen the interfacial interaction as well as influence the diffusion and release of aqueous monomer, providing a promising perspective on improving the stability and separation performance of TFNi membrane [28,29].

In this work, a novel TFNi NF membrane was fabricated by the IP reaction of piperazine and trimesoyl chloride, wherein the polydopamine decorated MXene (PDA@MXene) hybrid was introduced as an interlayer between PA barrier layer and polysulfone substrate. The membrane morphology, chemical composition, roughness, hydrophilicity, crosslinking degree and surface charge were systematically investigated. Based on the desalination test, PM-TFNi membrane demonstrated superior nanofiltration performance and structural stability, wherein the water flux was 18.3 L $m^{-2}$ $h^{-1}$ $bar^{-1}$, nearly 2 times as high as that of control TFC0 membrane, and the rejection of $Na_2SO_4$ maintained 98.0%.

## 2. Experimental

### 2.1. Materials and reagents

Polysulfone (PSF) substrate featuring with the pore size of 0.22 μm was purchased from Jialejing Membrane Technology Co., Ltd. (Nangjing, China). $Ti_3AlC_2$ (MAX) particles (≥ 99%, 300 mesh) were supplied by Mingshan Company (Nanjing, China). Trimesoyl chloride (TMC, 98%), piperazine (PIP, 99%) and n-hexane (97%), hydrochloric acid (HCl, 32%) and lithium fluoride (LiF, >99.0%), were bought from Sigma-Aldrich. Sodium sulfate ($Na_2SO_4$, 99%), magnesium sulfate ($MgSO_4$, 99%) and tris(hydroxymethyl)aminomethane (Tris) were supplied by Sinopharm Chemical Reagent Co., Ltd. (Shanghai, China). Magnesium chloride ($MgCl_2$, 99%), sodium chloride (NaCl, 99%), dopamine hydrochloride and polyethylene glycol (PEG, 200 −1000 Da) were provided by J&K Scientific (Beijing, China). Millipore water purification system was employed to supply the deionized (DI) water for the preparation of aqueous solutions.

### 2.2. Preparation of MXene nanosheets

MXene nanosheets were obtained by carrying out a mild in situ HF method reported in our previous work [21]. Concretely, LiF powder (3 g) was gradually poured into the 9 M of HCl solution (45 mL) with consecutive stirring. After the complete dissolution, $Ti_3AlC_2$ particles (3 g) were slowly added into the above in-situ etchant, and maintained at 35 °C for 24 h. Then, the acid mixture was rinsed by DI water to neutral pH under centrifugation at 3500 rpm for 5 cycles. The black sediment containing multilayer MXene was redispersed into 100 mL of DI water and subjected to the sonication for 45 min in flowing $N_2$ for further delamination. Finally, the above suspension was treated with the centrifugation at 3500 rpm for 30 min, and the uniform MXene colloidal solution was obtained for further use.

### 2.3. Preparation of polydopamine decorated MXene hybrid

To synthesize the polydopamine decorated MXene (PDA@MXene) hybrid, a certain amount of MXene (10, 20, 30 or 40 mg) was mixed with Tris-HCl buffer solution (10 mM, 100 mL) under continuous stirring, and the pH was adjusted to about 8.5 by diluted HCl solution. Subsequently, the obtained mixture was treated under sonication for 30 min for homogeneous dispersion. Dopamine (400 mg) was then added into above MXene-Tris-HCl mixture and followed by stirring for 1 h under dark condition. The obtained solution was centrifuged at 10,000 rpm under 4 ℃ for 30 min to get rid of the residues. Sediment containing PDA@MXene was collected and redispersed with 50 mL of DI water.

### 2.4. Fabrication of polyamide nanofiltration membranes

The PDA@MXene interlayered thin-film nanocomposite nanofiltration (PM-TFNi) membranes were fabricated through interfacial polymerization (IP), and the preparation procedure was illustrated in Fig. 1. Typically, the PSF substrates were immersed into DI water for 10 min before IP reaction. Then, the wet PSF substrates were fixed by the homemade plastic splint, and the PDA self-polymerization occurred after pouring the PDA@MXene solution onto the surface of PSF substrate. After reaction for 20 min, the residual PDA@MXene solution was removed with the aid of soft rubber. Next, the PIP aqueous solution (0.75 wt%) was poured on the PDA@MXene modified PSF (PM-PSF) surface and kept for 5 min. The excess PIP solution was gently wiped off. Afterwards, the organic TMC solution (0.038 wt%) was introduced on the PIP-soaked substrates for IP reaction and maintained for 30 s. The residual TMC solution was outwelled and the nascent-prepared TFNi membrane was immediately soaked into ID water to terminate the reaction. The resultant TFNi membrane was placed into DI water for further use. Additionally, the control TFC membrane and TFNi membrane with MXene as interlayer were prepared using the similar method without the introduction of PDA@MXene, which were named as TFC0 and MX-TFNi membrane, respectively.

### 2.5. Characterizations

Morphologies of MXene nanosheets and PDA@MXene hybrid were characterized by high-resolution transmission electron microscopy (HRTEM, FEI Tecnai G2 F20, Japan). The crystallographic information of nanomaterial samples was detected by the X-ray diffraction (XRD) analysis over the $2\theta$ range of 5 to 70°with the scanning rate of 0.2 s $step^{-1}$. Fourier transform infrared spectroscopy (FTIR, TENSOR 27, Bruker, Germany) was applied to investigate the near-surface functional groups of samples within a scanning range of 100–4000 $cm^{-1}$.

the surface and cross-section micrographs of all membranes were visualized by the field emission scanning electron microscope (FESEM, Hitachi S4800, Japan). The Energy Dispersive Spectrometer (EDS, Oxford Instrument with JED-2300 Analysis Station) equipped on FESEM was employed to analyze the elemental distribution on the substrate. Note that the samples should be subjected to sputter-coating with gold before FESEM and EDS observation. Atomic force microscopy (AFM, NSG10, NT-MDT, ca. 330 kHz) was further employed to assess the membrane surface roughness. Water contact angles were tested on a contact angle measurement system (CAM200) to evaluate the hydrophilcity of membrane surface. The Anton Paar SurPASS electrokinetic analyzer was used to detect the zeta potential of the as-prepared NF membranes by using KCl aqueous solution (1 mM, pH=3.0–10.0). The chemical structure and element component of the NF membranes were investigated via the X-ray photoelectron spectrometer (XPS, Thermo Fisher ESCALAB 250, USA) equipped with the monochromatic 100-eV Al-Kα X-ray source. It was worth noting that all samples were thoroughly dried at 25 ℃ for 12 h prior to characterization.

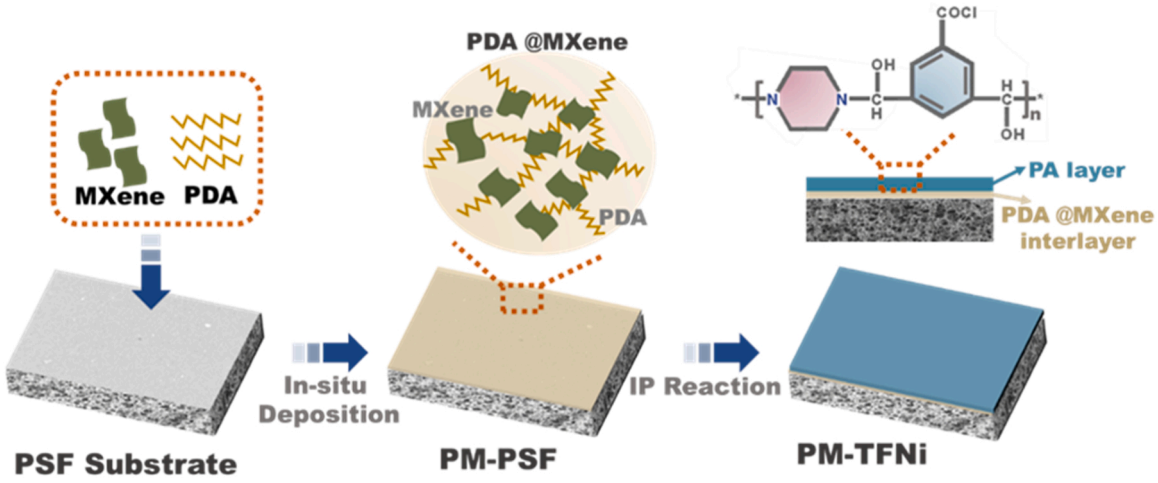


**Fig. 1.** Schematic of the fabrication of the PDA@MXene interlayered thin-film nanocomposite nanofiltration membrane.

To calculate the water uptake of substrates, the membranes were soaked in deionized (DI) water for a duration of 24 h. Afterward, the residual water on the membrane surface was carefully removed by wiping, and the weight of the membranes was immediately measured. Water uptake was estimated by Eq. (1).

$$Water \quad uptake = \frac{w_u - w_s}{w_s} \times 100\% \tag{1}$$

Where $w_u$ is the weight of wet membrane, while $w_s$ is the weight of dry membrane.

### 2.6. Evaluation of nanofiltration performance

The desalination performances (water flux and salt rejection) of the NF membranes were measured by employing a homemade cross-flow filtration setup with the effective separation area of 34 $cm^2$, as reported in previous work [19]. For compaction, the NF membranes were pre-filtrated using DI water with the fixed pressure of 5 bar for 30 min. Subsequently, the water flux (J, L $m^{-2}$ $h^{-1}$ $bar^{-1}$) was estimated by the mass change of the filtrated solution over time, which can be calculated by Eq. (2).

$$A = \frac{V}{S \times P \times t} \tag{2}$$

where V represents the volume of the filtrated solution (L), S represents the effective membrane area ($m^2$), p represents the operation pressure (bar), and t represents the collection interval during the nanofiltration test.

Salt rejections (R, %) of the as-prepared membranes were measured using a single type of salt (($NaSO_4$, $MgSO_4$, $MgCl_2$ and NaCl) with the concentration of 2000 ppm, which can be calculated through Eq. (3).

$$R(\%) = \left(1 - \frac{C_p}{C_f}\right) \times 100\% \tag{3}$$

where $C_f$ and $C_p$ represent the salt concentrations of the feed and filtrated solution, respectively, which were evaluated by the conductivity meter.

The selectivity ($S_{A/B}$) of NF membranes was measured using two types of salts, which can be calculated using Eq. (4).

$$S_{\frac{A}{B}} = \frac{1 - R_A}{1 - R_B} \tag{4}$$

where $R_A$ and $R_B$ are the retention rate of salt A and salt B, respectively.

## 3. Results and discussion

### 3.1. Characterization of MXene based materials

The HRTEM micrographs in Fig. 2 displayed the topological structure of the MXene based materials. It is obvious that the ultrathin MXene nanosheets shows nearly transparent and flat surface, which is in accordance with the previous reports (Fig. 2a) [30,31]. After the modification, the PDA was clearly observed on the MXene surface and the stratified structure of MXene was well maintained (Fig. 2b), which also could be confirmed by the Tyndall effect of PDA@MXene colloidal solution. Remarkably, the color of the MXene solution turned from atrovirens to golden, manifesting the successfully decoration of PDA on MXene nanosheets due to the robust adhesion capability (Fig.S1).

### 3.2. Characterization of PDA@MXene modified substrate

The physicochemical characteristic of the PDA@MXene modified PSF substrate was further investigated. SEM images in Fig. 2c-e demonstrated that the surface of all modified substrate became rougher compared to that of control PSF substrate. Furthermore, only C, O and S elements were detected on the pristine PSF surface, while Ti and F elements with uniform distribution were present on the MXene modified PSF substrate (MX-PSF) (Figs. S2-S3). After loaded with PDA@MXene hybrid, N element were also observed deriving from the -$NH_2$ group of PDA (Fig. S4). These results reveal the successful coverage of MXene nanosheets or PDA@MXene hybrid on the PSF substrate. The FTIR spectra in Fig. 2f shows the typical peaks centered at 1330–1290 and 1180–1150 $cm^{-1}$ were ascribed to the asymmetric and symmetric S-O stretching vibrations in PSF substrate[32]. After modification, a new peak centered at 1615 $cm^{-1}$ appeared in the PDA@MXene modified PSF substrate (PM-PSF), attributing to bending vibration of N–H and stretching vibration of C-C in aromatic ring of PDA [29], which further confirm the successful introduction of PDA@MXene hybrid. Additionally, the surface zeta potential of PSF, MX-PSF and PM-PSF substrate were − 13.8, − 14.5 and − 19.7 mV, respectively. (Fig.S5) Fig. 2g illustrates the surface hydrophilicity and water uptake of the substrates. The water contact angles of control PSF, MX-PSF and PM-PSF substrates were 83.4°, 74.3° and 70.1°, respectively, suggesting that the PDA@MXene layer has superior hydrophilicity, which was ascribed to the considerable hydrophilic groups in PDA@MXene (including catechol, imine and quinone groups from PDA, and hydroxyl group from MXene). In this way, the water uptake enhanced from 29.5% of PSF to 45.6% of PM-PSF substrates. This was mainly because there was strong hydrogen bonding between those hydrophilic groups and water,

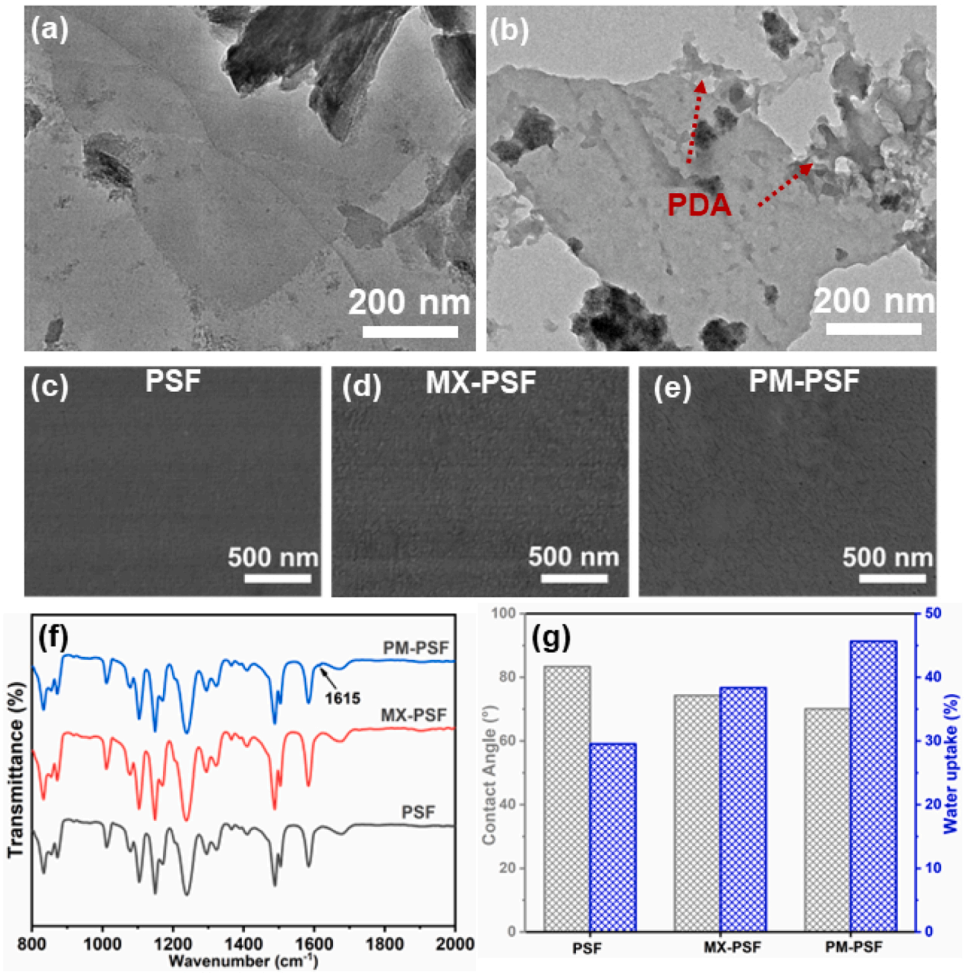


**Fig. 2.** Characterization of the MXene based materials and the modified substrates. HRTEM images of (a) MXene nanosheets and (b) PDA@MXene hybrid. SEM images of (c) pristine PSF, (d) MX-PSF and (e) PM-PSF substrate. (f) FTIR spectra of different substrates. (g) Water contact angles and water uptake of different substrates.

boosting the adsorption of water molecules to the PDA@MXene layer, which could accelerate the storage of the amine monomers during the IP process [4,26]. It can be insinuated the introduction of MXene or PDA@MXene layer could prominently change the surface properties of the substrate, which plays an essential role in the preparation of the nanofiltration membrane with outstanding performance.

### *3.3. Characterization of the polyamide nanocomposite nanofiltration membranes*

The polyamide layer was formed by performing the IP reaction on the top surface of control and modified surface. The surface and sectional morphologies of the obtained nanofiltration membranes was observed by SEM mages. Fig. 3 illustrates that the TFC0 membrane showed a nearly flat surface with scattered granular globules. For comparison, MX-TFNi membrane exhibited a rougher and more heterogeneous polyamide layer with abundant protuberances, which was probably because the MXene nanosheets with hydrophilic feature offered more reaction area and accelerated the adsorption of piperazine monomers, essentially resulting in the rapid reaction rate of IP process and the transformation of membrane surface morphology. Along with the deposition of PDA@MXene nanosheets, the nodule-like nanostructure PM-TFNi membrane became more obvious and intensive compared to that of MX-TFNi membrane. This phenomenon could be primarily ascribed to the further enhanced hydrophilicity of modified substrate.

Fig. 3b shows that the thicknesses of the selective PA layers were 160, 90 and 40 nm for TFC0, MX-TFNi and PM-TFNi membrane respectively. On the basis of the Freger's kinetic model [33], the thinnest PA layer of PM-TFNi membrane was mainly derived from the strengthened interaction between the amine monomers and the hydrophilic groups (such as carbonyl groups, secondary amine and hydroxyl groups) on PDA and MXene nanosheets, thus impeding the diffusion of PIP monomer as well as the reaction with the organic phase.

AFM images in Fig. 3c displays the surface roughness of the NF membranes. As is shown, PM-TFNi membrane presented the roughest surface with the $R_a$ value of 10.06 nm, which was approximately 3 times compared with that of TFC0 membrane, agreeing well with the results of SEM images. Generally, the rougher surface would potentially increase the permeable area on the PA layer, which was conductive to the efficient transport of water molecules and improving the water flux.

The surface functional groups of the NF membranes were further investigated by FTIR analysis. It is clearly unraveled in Fig. 4a that the peak at 1630 $cm^{-1}$ was assigned to the stretching -C═O bond in the amide group [34]. At the same time, a broad peak at approximately 3454 $cm^{-1}$ was also observed, which was corresponding to the stretching vibration of -OH and -NH groups from the hydrolysis TMC and PIP, respectively [35]. These results verified the successful formation of the selective PA layer on the substrate. It is noteworthy that above two peaks of MX-TFNi and PM-TFNi membranes became weak relative to that of TFC0 membrane, which was probably because of the decreased thickness of PA layer [36].

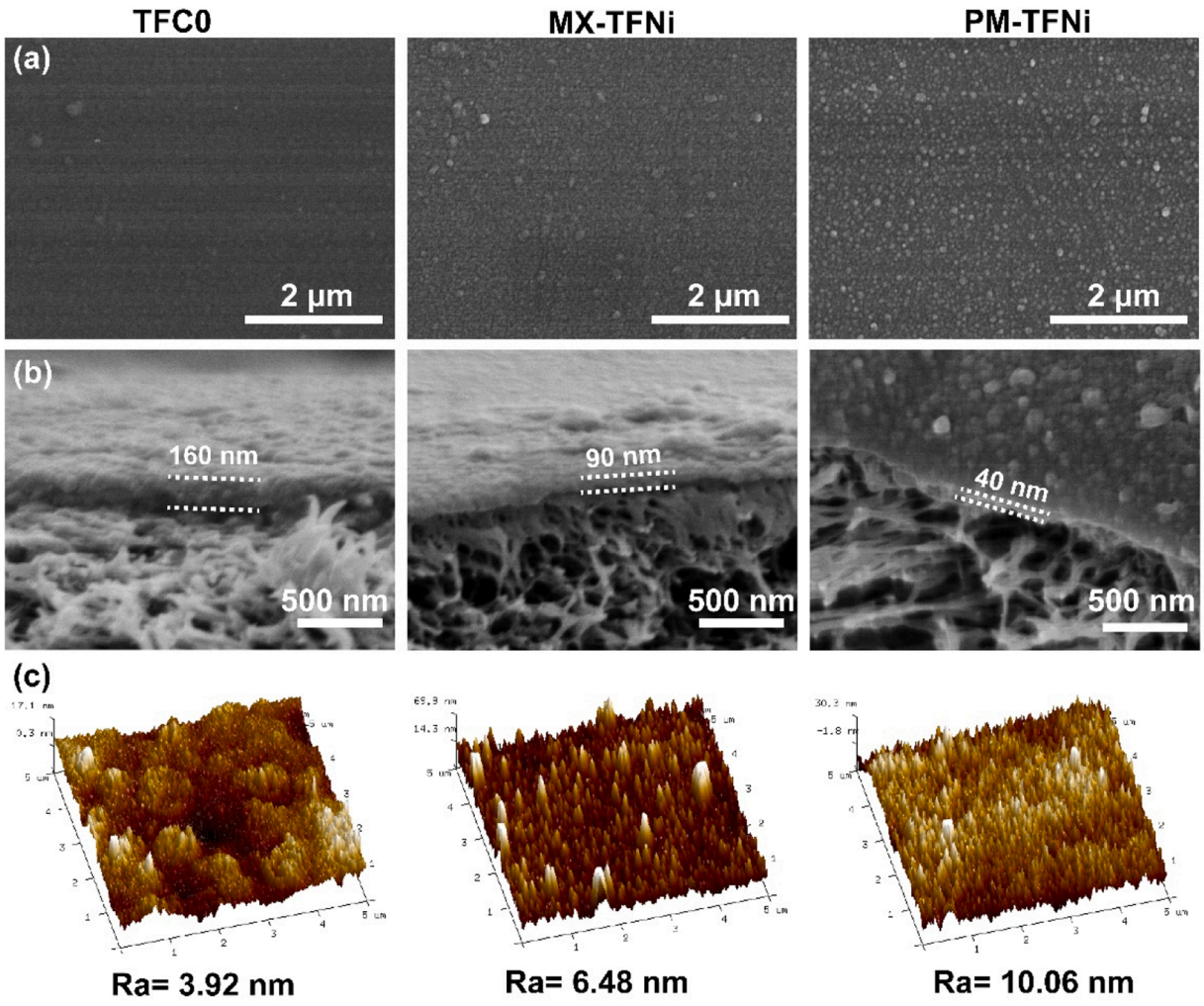


**Fig. 3.** Morphological characterizations of membranes. SEM images of the (a) surface section and (b) cross section of TFC0, MX-TFNi, PM-TFNi membranes, respectively. (c) AFM images of TFC0, MX-TFNi and PM-TFNi membrane, respectively.

The element component and chemical bonding of the membrane surface were analyzed by the XPS measurement. Fig. 4b depicted all as-fabricated NF membranes exhibited three distinct peaks assigned to C, N and O elements. According to the elemental atomic percentages of N and O on the membrane surface, the crosslinking degree was estimated and displayed in Table 1. The result shows that the crosslinking degree of NF membranes significantly elevated with the introduction of MXene (65.57%) and PDA@MXene (72.77%) interlayer compared to that of TFC0 membrane (47.93%). More cross-linked PA layer signified a denser structure, which would significantly contribute to the superior desalination performance of NF membrane. Three peaks compositions at the binding energies about 287.6, 285.7 and 284.6 eV were involved in the high-resolution XPS C1s spectra of all NF membranes, which are attributed to N-C═O, C-N and C-C, respectively [37]. Furthermore, O1s spectra could be divided into two peaks at binding energies of 532.0 and 530.5 eV, corresponding to O-C═O and O-C═N, respectively. These results reveal the IP process underwent successfully[38].

The water contact angles (CA) in Fig. 5a were used to determine the surface hydrophilicity of the NF membranes. Obviously, the CA values decreased from 47.8° of TFC0 to 41.3° and 39.7° for MX-TFNi and PM-TFNi membrane, respectively, elucidating a more hydrophilic surface was obtained after the modification of substrate by MXene or PDA@MXene. As is well known, the CA value was mainly affected by the surface free energy and roughness of the membrane. On the one hand, the surface free energy was almost unchanged as the chemical components of all surfaces of the NF membranes were polyamide. On the other hand, according to the Cassie theory, the water CA would reduce with the increasement of the surface roughness, which primarily contributed to the lower CA value of PM-TFNi membrane[23].

Surface charge of the NF membrane is considered as a crucial parameter affecting the salt rejection through the Donnan effect. Zeta potential analysis was carried out within the pH range of 3–10 to evaluate the surface charge property. It can be observed from Fig. 5b that the zeta potentials of all membranes gradually diminished with the increase of pH value, and became negative when the pH over 4. Moreover, the zeta potentials dropped slightly with the introduction of interlayers, and PM-TFNi membrane exhibited the most negatively charged surface, which would be beneficial to the repulsion of anions during the nanofiltration process. It is generally recognized that the negative surface of the selective layer is derived from the generation of carboxyl group by the hydrolysis of aryl chloride group on the unreacted TMC monomer [39]. As for PM-TFNi membrane, the PDA@MXene interlayer improved the concentration of PIP monomer on the modified substrate and boosted the incipient PA layer formation, which hampered the subsequent diffusion of the PIP monomer, thereby resulting in more residual TMC monomer.

The molecular weight cutoffs (MWCOs) of the NF membranes were measured through performing a series of filtration experiments using PEG polymers (range of the molecular weight: 200 - 800 Da) as the model solutes, and the result was shown in Fig. 5c. It can be seen that the

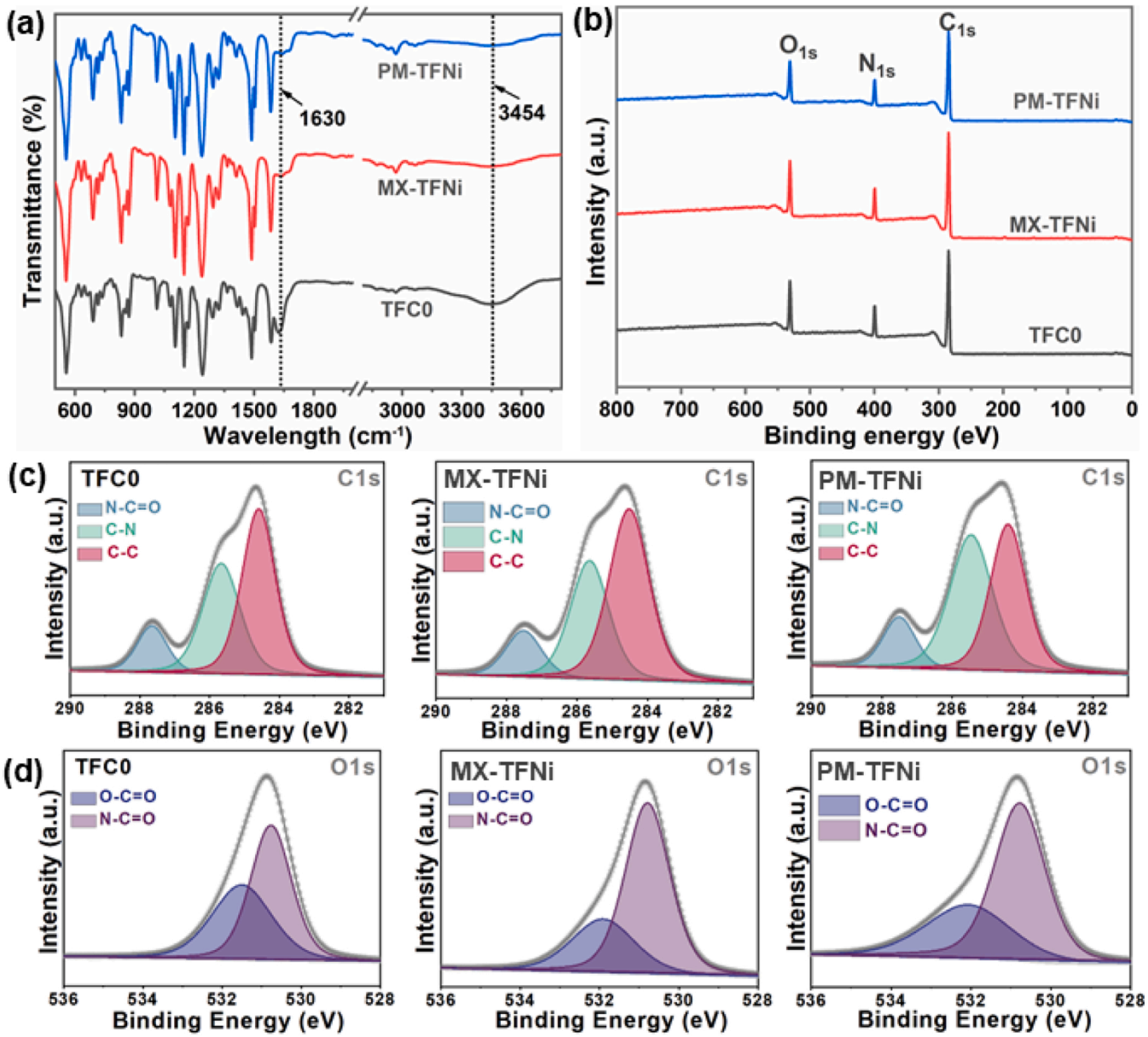


**Fig. 4.** Surface chemical structures of the NF membranes. (a) FTIR spectra, (b) XPS survey spectra, High-resolution XPS spectra of (c) C1s and (d) O1s of TFC0, MX-TFNi, PM-TFNi membranes, respectively.

**Table 1**
Surface element compositions of NF membranes and the relative crosslinking degree.

| Membrane | Atomic percentage in XPS (%) | | | O/N | Crosslinking degree (%) |
|---|---|---|---|---|---|
| | C | O | N | | |
| TFC0 | 75.9 | 14.08 | 10.02 | 1.41 | 47.93 |
| MX-TFNi | 74.56 | 14.18 | 11.26 | 1.26 | 65.57 |
| PM-TFNi | 71.91 | 15.32 | 12.77 | 1.2 | 72.77 |

MWCOs of TFC0, MX-TFNi and PM-TFNi membrane were 394, 386 and 378 Da, respectively, suggesting that PM-TFNi membrane possessed the densest selective layer, which is in accordance with the result of XPS analysis.

### 3.4. Nanofiltration performance of membranes

The nanofiltration performances of the as-fabricated membranes were studied with respect to the water permeance and salt rejection testing by the cross-flow device. In order to determine the optimal preparation parameters of PX-TFNi membranes, the influences of the mass ratio of PDA and MXene nanosheets as well as the deposition time of PDA@MXene interlayer on the nanofiltration performance were systematically investigated. The results in Fig.S6 show when the mass ratio of MXene nanosheets and PDA was 1:25 and the deposition time was 20 min, the PM-TFNi membrane exhibited the optimized performance, wherein the water flux was 18.3 L $m^{-2}$ $h^{-1}$ $bar^{-1}$, nearly 2 and 1.3 times higher than that of TFC0 membrane (9.17 L $m^{-2}$ $h^{-1}$ $bar^{-1}$) and MX-TFNi membrane (14.40 L $m^{-2}$ $h^{-1}$ $bar^{-1}$), respectively, and the rejection of $Na_2SO_4$ reached astonishing 98.0% (Fig. 6a). There are several reasons contributing to the superior permeability of PM-TFNi membrane: (i) the decreased thickness of the selective PA layer would shorten the channel length and reduce the transmission resistance of water molecules. (ii) The rougher surface of the PM-TFNi membrane would offer larger effective filtration area and more transport paths. (iii) The gutter effect caused by the interlayer effectually minimized the

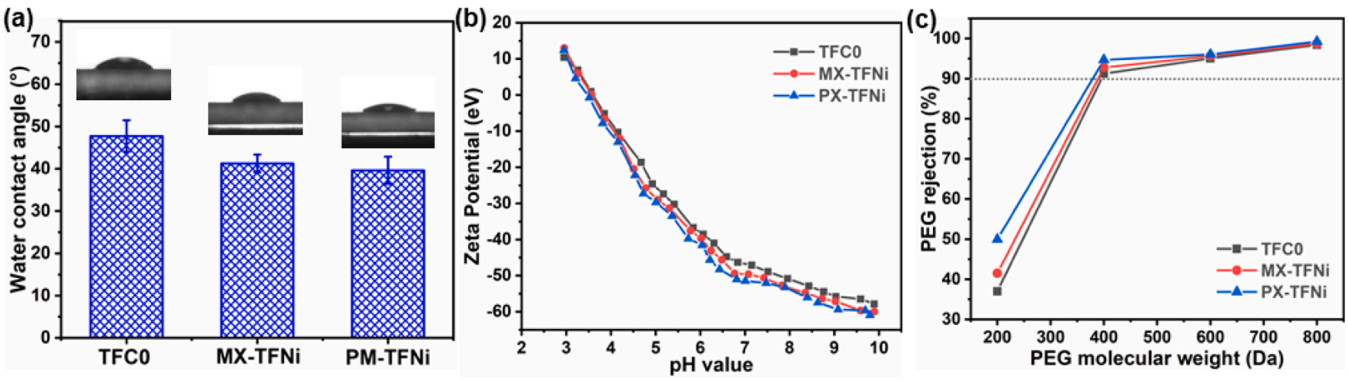


**Fig. 5.** (a) Water contact angles, (b) Zeta potentials and (c) Molecular weight cutoffs of TFC0, MX-TFNi, PM-TFNi membranes.

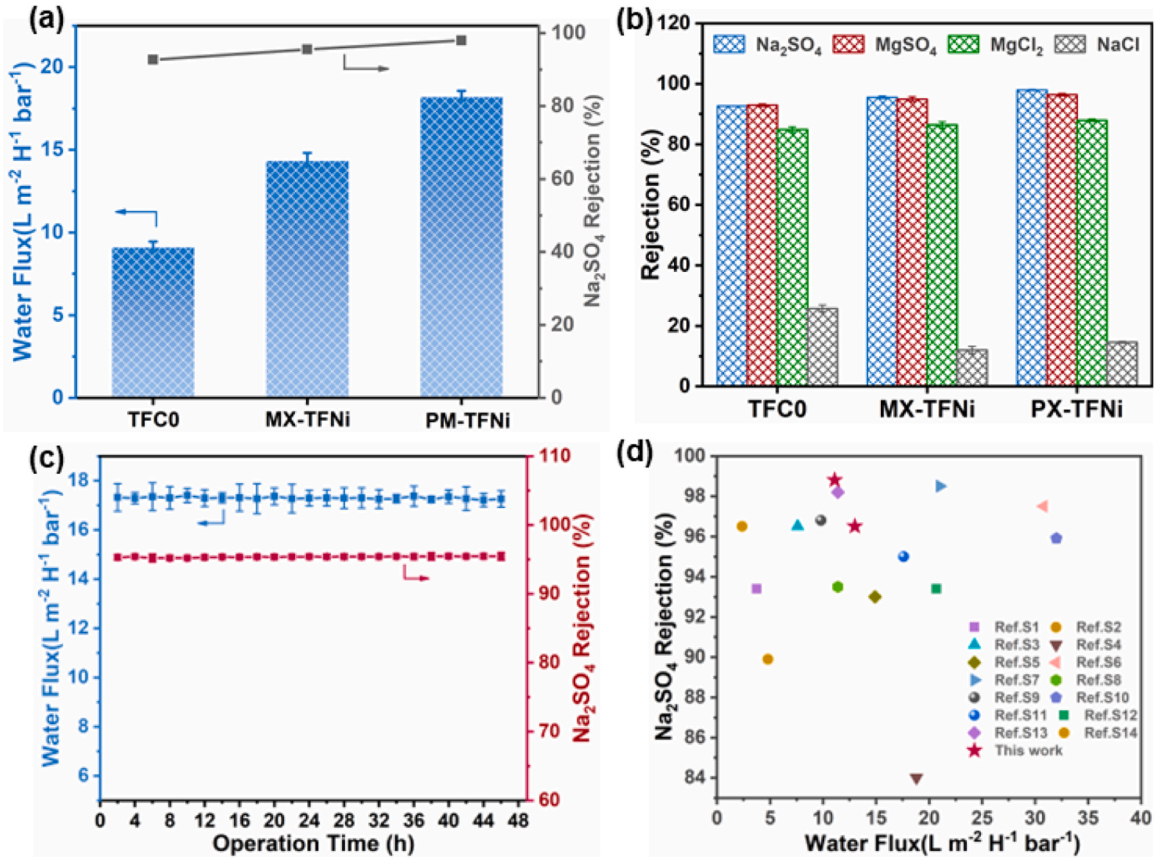


**Fig. 6.** (a) Water flux and $Na_2SO_4$ rejection of the NF membranes. (b) Rejections of different salts of NF membranes (Concentration of salt solution is 2000 ppm). (c) Long-term stability of PM-TFNi membrane. (d) Rejection for $Na_2SO_4$ in different pH values of the PM-TFNi membrane.

transversal water transportation and elevate the water permeance [40]. Meanwhile, the higher selectivity of the PM-TFNi membrane was mainly ascribed to its denser PA layer with higher crosslinking degree and the more negatively charged surface, accelerating the rejection of salt ions.

The selective behavior of NF membranes towards four different salt solutions was comprehensively investigated. It is obvious from Fig. 6b that the inorganic salt retention of different membranes reduced following the similar tendency: $Na_2SO_4$ > $MgSO_4$ >$MgCl_2$ >NaCl, which is deemed to the typical separation performance of negatively charged NF PA membranes [41,42]. Obviously, the NF membranes exhibited higher rejection towards the salt solutions containing divalent anions and monovalent cations due to the synergistic Donnan effect and size screening effect. Moreover, PM-TFNi membrane presented the higher rejection of $Na_2SO_4$, $MgSO_4$ and $MgCl_2$ over that of TFC0 and MX-TFNi membranes, deriving from the formation of the denser and more negatively charged selective PA layer. Unexpectedly, the NaCl rejections of the TFNi NF membranes were lower rather than higher as in the case of multivalent salts, which was primarily because that the density of the PA layer had negligible influence on the penetrability of salt with relatively small hydration radius, leading to the readily transport of NaCl through the thinner barrier layer along with water molecules. The selectivity of monovalent/divalent salt was hereby calculated and shown in Table S1. PM-TFNi had the highest values of $S_{NaCl/Na2SO4}$, $S_{NaCl/MgSO4}$ and $S_{NaCl/MgCl2}$, demonstrating that the introduction of PDA@MXene interlayer would be beneficial to the practical application of water desalination. Furthermore, it can be concluded from the summarized data in Fig. 6d and Table S2 that the permeability and selectivity of PM-TFNi membrane is comparable to or better than many other reported NF

membranes.

The chemical and mechanical stability is prerequisite for the practical application of NF membrane. Long-term stability of PM-TFNi membrane tested with 2000 ppm $Na_2SO_4$ solution were shown in Fig. 6c, and it is found that the water flux and salt rejection of PM-TFNi membrane maintained stable after 48 h operation. Additionally, the pH resistance of PM-TFNi membrane was determined through measuring its separation property after immersing into the solutions with the pH values of 3, 7 and 11 for 24 h, respectively. Fig.S7 indicates that no obvious changes in the water flux and salt retention for PM-TFNi membrane were observed after acid or alkaline treatment. The excellent long-term stability and pH resistance could endow the PM-TFNi membrane with effective and durable separation process in harsh conditions for a long time.

## 4. Conclusions

In summary, a novel TFNi NF membrane was successfully fabricated by introducing the PDA@MXene interlayer on the PSF substrate to regulate the IP process. The improved adsorption and constrained diffusion of amine monomers caused by the high-density uptake capability of PDA@MXene layer promoted the formation of granular PA layer with thinner thickness, rougher surface, denser structure, better hydrophilicty and more negatively charged surface, which be beneficial to the significantly enhancement in the permeability without compromising selectivity. Moreover, the PM-TFNi membrane demonstrated excellent pH resistance and excellent structural stability in long-term operation. Therefore, PM-TFNi membrane could be a promising candidate for the practical application of desalination.

## CRediT authorship contribution statement

**Yuyang Wu**: Methodology, Data curation, Writing – original draft preparation. **Chen Yao**: Conceptualization, Methodology, Software. **Yuanyuan Wang**: Software, Validation. **Mingmei Ding**: Supervision, Funding acquisition. **Hang Xu**: Software, Validation. **Hang Xu**: Software, Validation. **Li Gao**: Writing – review & editing.

## Declaration of Competing Interest

The authors declare the following financial interests/personal relationships which may be considered as potential competing interests: Mingmei Ding reports financial support was provided by Fundamental Research Funds for the Central Universities. Mingmei Ding reports financial support was provided by National Natural Science Foundation of China. Hang Xu reports was provided by National Natural Science Foundation of China. Mingmei Ding reports financial support was provided by Natural Science Foundation of Jiangsu Province.

## Data availability

Data will be made available on request.

## Acknowledgements

This work was financially supported by the Key-Area Research and Development Program of Guangdong Province (2020B0101130001), Natural Science Foundation of Jiangsu Province (BK20220989) and National Natural Science Foundation of China (52200011 and 51978239).

## Appendix A. Supporting information

Supplementary data associated with this article can be found in the online version at doi:10.1016/j.jece.2024.111963.

## References

[1] J. Garcia-Ivars, L. Martella, M. Massella, C. Carbonell-Alcaina, M.I. Alcaina-Miranda, M.I. Iborra-Clar, Nanofiltration as tertiary treatment method for removing trace pharmaceutically active compounds in wastewater from wastewater treatment plants, Water Res 125 (2017) 360–373.
[2] L. Gao, G. Yang, J.H. Zhang, Z.L. Xie, De-ammonification using direct contact membrane distillation -An experimental and simulation study, Sep. Purif. Technol. 250 (2020) 117158.
[3] M. Ding, H. Xu, C. Yao, W. Chen, N. Song, Q. Zhang, T. Lin, Z. Xie, Understanding the membrane fouling control process at molecular level in the heated persulfate activation- membrane distillation hybrid system, Water Res 229 (2023) 119465.
[4] H. Xu, Q. Zhang, N.H. Song, J.P. Chen, M.M. Ding, C.H. Mei, Y.C. Zong, X.Y. Chen, L. Gao, Membrane distillation by novel Janus-enhanced membrane featuring hydrophobic-hydrophilic dual-surface for freshwater recovery, Sep. Purif. Technol. 302 (2022) 122036.
[5] Y. Liang, Y. Zhu, C. Liu, K.R. Lee, W.S. Hung, Z. Wang, Y. Li, M. Elimelech, J. Jin, S. Lin, Polyamide nanofiltration membrane with highly uniform sub-nanometre pores for sub-1 A precision separation, Nat. Commun. 11 (2020) 2015.
[6] A. Wang, H. Xu, J.W. Fu, T. Lin, J. Ma, M.M. Ding, L. Gao, Enhanced high-salinity brines treatment using polyamide nanofiltration membrane with tunable interlayeredMXene channel, Sci. Total Environ. 856 (2023) 158434.
[7] P. Sarkar, S. Modak, S. Karan, Ultraselective and highly permeable polyamide nanofilms for ionic and molecular nanofiltration, Adv. Func, Mater 31 (2020) 2007054.
[8] Y. Chen, H. Sun, S. Tang, H. Feng, H. Zhang, K. Chen, P. Li, Q.J. Niu, Nanofiltration membranes with enhanced performance by constructing an interlayer integrated with dextran nanoparticles and polyethyleneimine coating, J. Membr. Sci. 654 (2022) 120537.
[9] S. Gao, Y. Zhu, Y. Gong, Z. Wang, W. Fang, J. Jin, Ultrathin polyamide nanofiltration membrane fabricated on brush-painted single-walled carbon nanotube network support for ion sieving, ACS Nano 13 (2019) 5278–5290.
[10] F. Wang, Z. Yang, C.Y. Tang, Modeling water transport in interlayered thin-film nanocomposite membranes: Gutter effect vs Funnel effect, ACS Environ. Sci. Technol. Eng. 2 (2022) 2023–2033.
[11] Z. Zha, P. He, S. Zhao, R. Guo, Z. Wang, J. Wang, Interlayer-modulated polyamide composite membrane for organic solvent nanofiltration, J. Membr. Sci. 647 (2022) 120306.
[12] M.X. Liu, W. Chen, J.W. Fu, A.Q. Wang, M.M. Ding, L. Zhang, L. Han, L. Gao, Hyaluronic acid-modified nanofiltration membrane for ultrahigh water permeance and efficient rejection of PFASs, Process Saf. Environ. 166 (2022) 214–221.
[13] Y. Lu, R. Wang, Y. Zhu, Z. Wang, W. Fang, S. Lin, J. Jin, Two-dimensional fractal nanocrystals templating for substantial performance enhancement of polyamide nanofiltration membrane, Proc. Natl. Acad. Sci. USA 118 (2021) e2019891118.
[14] J. Wu, M. Xia, Z. Li, L. Shen, R. Li, M. Zhang, Y. Jiao, Y. Xu, H. Lin, Facile preparation of polyvinylidene fluoride substrate supported thin film composite polyamide nanofiltration: Effect of substrate pore size, J. Membr. Sci. 638 (2021) 119699.
[15] Y. Kang, M. Obaid, J. Jang, I.S. Kim, Sulfonated graphene oxide incorporated thin film nanocomposite nanofiltration membrane to enhance permeation and antifouling properties, Desalination 470 (2019) 114125.
[16] D. Xu, X. Zhu, X. Luo, Y. Guo, Y. Liu, L. Yang, X. Tang, G. Li, H. Liang, MXene nanosheet templated nanofiltration membranes toward ultrahigh water transport, Environ. Sci. Technol. 55 (2021) 1270–1278.
[17] Z. Yang, Y. Wu, J. Wang, B. Cao, C.Y. Tang, In situ reduction of silver by polydopamine: A novel antimicrobial modification of a Thin-film composite polyamide membrane, Environ. Sci. Technol. 50 (2016) 9543–9550.
[18] B. Anasori, M.R. Lukatskaya, Y. Gogotsi, 2D metal carbides and nitrides (MXenes) for energy storage, Nature Rev, Mater 2 (2017) 16098.
[19] J. Ma, Y. Wang, H. Xu, M. Ding, L. Gao, MXene ($Ti_3T_2C_X$)-reinforced thin-film polyamide nanofiltration membrane for short-chain perfluorinated compounds removal, Process Saf. Environ. 168 (2022) 275–284.
[20] L. Ding, L. Li, Y. Liu, Y. Wu, Z. Lu, J. Deng, Y. Wei, J. Caro, H. Wang, Effective ion sieving with $Ti_3C_2T_x$ MXene membranes for production of drinking water from seawater, Nat. Sustain 3 (2020) 296–302.
[21] H. Xu, J. Ma, M. Ding, Z. Xie, Mechanistic insights into the removal of PFOA by 2D MXene/CNT membrane with the influence of $Ca^{2+}$ and humic acid, Desalination 529 (2022) 115643.
[22] X. Wu, M. Ding, H. Xu, W. Yang, K. Zhang, H. Tian, H. Wang, Z. Xie, Scalable $Ti_3C_2T_x$ MXene interlayered forward osmosis membranes for enhanced water purification and organic solvent recovery, ACS Nano 14 (2020) 9125–9135.
[23] J. Fu, H. Xu, T. Lin, A. Wang, A. Wang, C. Yao, W. Chen, M. Ding, C. Geng, L. Gao, Tailoring the crumpled structures of a polyamide membrane with a heterostructural MXene-$TiO_2$ interlayer for high water permeability, Desalination 549 (2023) 116352.
[24] P.F. Sun, Z. Yang, X. Song, J.H. Lee, C.Y. Tang, H.D. Park, Interlayered forward osmosis membranes with $Ti_3C_2T_x$ MXene and carbon nanotubes for enhanced municipal wastewater concentration, Environ. Sci. Technol. 55 (2021) 13219–13230.
[25] M. Wu, J. Yuan, H. Wu, Y. Su, H. Yang, X. You, R. Zhang, X. He, N.A. Khan, R. Kasher, Z. Jiang, Ultrathin nanofiltration membrane with polydopamine-covalent organic framework interlayer for enhanced permeability and structural stability, J. Membr. Sci. 576 (2019) 131–141.
[26] Y. Wang, T. Wang, S. Li, Z. Zhao, X. Zheng, L. Zhang, Z. Zhao, Novel Poly (piperazinamide)/poly(m-phenylene isophthalamide) composite nanofiltration

membrane with polydopamine coated silica as an interlayer for the splendid performance, Sep. Purif. Technol. 285 (2022) 120390.
[27] Q. Shen, Y. Lin, T. Ueda, P. Zhang, Y. Jia, T. Istirokhatun, Q. Song, K. Guan, T. Yoshioka, H. Matsuyama, The underlying mechanism insights into support polydopamine decoration toward ultrathin polyamide membranes for high-performance reverse osmosis, J. Membr. Sci. 646 (2022) 120269.
[28] T. Wang, J. Wang, Z. Zhao, X. Zheng, J. Li, H. Liu, Z. Zhao, Bio-inspired fabrication of anti-fouling and stability of nanofiltration membranes with a poly(dopamine)/graphene oxide interlayer, Ind. Eng. Chem. Res 60 (2021) 14868–14883.
[29] B. Zhao, X. Long, H. Wang, L. Wang, Y. Qian, H. Zhang, C. Yang, Z. Zhang, J. Li, C. Ma, Y. Shi, Polyamide thin film nanocomposite membrane containing polydopamine modified ZIF-8 for nanofiltration, Colloid Surf. A 612 (2021) 125971.
[30] M. Ding, H. Xu, W. Chen, G. Yang, Q. Kong, D. Ng, T. Lin, Z. Xie, 2D laminar maleic acid-crosslinked MXene membrane with tunable nanochannels for efficient and stable pervaporation desalination, J. Membr. Sci. 600 (2020) 117871.
[31] Y. Kang, Y. Xia, H. Wang, X. Zhang, 2D laminar membranes for selective water and ion transport, Adv. Func. Mater. 29 (2019) 1902014.
[32] X. Zhang, Y. Lv, H.C. Yang, Y. Du, Z.K. Xu, Polyphenol coating as an interlayer for thin-film composite membranes with enhanced nanofiltration performance, ACS Appl. Mater. Interfaces 8 (2016) 32512–32519.
[33] N. Fridman-Bishop, V. Freger, What makes aromatic polyamide membranes superior: New insights into ion transport and membrane structure, J. Membr. Sci. 540 (2017) 120–128.
[34] S. Gholami, J. López, A. Rezvani, V. Vatanpour, J.L. Cortina, Fabrication of thin-film nanocomposite nanofiltration membranes incorporated with aromatic amine-functionalized multiwalled carbon nanotubes. Rejection performance of inorganic pollutants from groundwater with improved acid and chlorine resistance, Chem. Eng. J. 384 (2020) 123348.
[35] H. Lan, Y. Zhai, K. Chen, Z. Zhai, C. Jiang, P. Li, Y. Hou, Q. Jason, Niu, Fabrication of high performance nanofiltration membrane by construction of Noria based nanoparticles interlayer, Sep. Purif. Technol. 290 (2022) 120781.
[36] B. Li, X.-X. Ke, Z.-H. Yuan, L.-B. Zhong, Q.-B. Zhao, Y.-M. Zheng, High performance electrospun thin-film composite forward osmosis membrane by tailoring polyamide active layer with polydopamine interlayer for desulfulrization wastewater desalination, Desalination 534 (2022) 115385.
[37] S. Karan, Z. Jiang, L.A.G. Sub-10, nm polyamide nanofilms with ultrafast solvent transport for molecular separation, Science 348 (2015) 1347–1351.
[38] L. Bai, Y. Liu, N. Bossa, A. Ding, N. Ren, G. Li, H. Liang, M.R. Wiesner, Incorporation of cellulose nanocrystals (CNCs) into the polyamide layer of thin-film composite (TFC) nanofiltration membranes for enhanced separation performance and antifouling properties, Environ. Sci. Technol. 52 (2018) 11178–11187.
[39] P. Hu, B. Tian, Z. Xu, Q. Jason, Niu, Fabrication of high performance nanofiltration membrane on a coordination-driven assembled interlayer for water purification, Sep. Purif. Technol. 235 (2020) 116192.
[40] Z. Yang, F. Wang, H. Guo, L.E. Peng, X.H. Ma, X.X. Song, Z. Wang, C.Y. Tang, Mechanistic insights into the role of polydopamine interlayer toward improved separation performance of polyamide nanofiltration membranes, Environ. Sci. Technol. 54 (2020) 11611–11621.
[41] J. Chen, Z. Li, C. Wang, H. Wu, G. Liu, Synthesis and characterization of g-C3N4 nanosheet modified polyamide nanofiltration membranes with good permeation and antifouling properties, RSC Adv. 6 (2016) 112148–112157.
[42] N. Izadmehr, Y. Mansourpanah, M. Ulbricht, A. Rahimpour, M.R. Omidkhah, TETA-anchored graphene oxide enhanced polyamide thin film nanofiltration membrane for water purification; performance and antifouling properties, J. Environ. Manag. 276 (2020) 111299.